Sensors and Actuators B 230 (2016) 592–599

Contents lists available at ScienceDirect

Sensors and Actuators B: Chemical

journal homepage: www.elsevier.com/locate/snb

The influence of nonstoichiometry on electrical transport and ethanol sensing characteristics for nanocrystalline $LaFe_xO_{3-\delta}$ sensors

Kang Cao, Ensi Cao*, Yongjia Zhang, Wentao Hao, Li Sun, Hua Peng

Key Lab. Of Advance Transducres & Intelligent Control System, College of Physics & Optoelectronics, Taiyuan University of Techonology, Taiyuan 030024, People's Republic of China

ARTICLE INFO

Article history:
Received 3 September 2015
Received in revised form 7 February 2016
Accepted 19 February 2016
Available online 26 February 2016

Keywords:
Nonstoichiometry
$LaFeO_3$
XPS
Sensing mechanism
Gas sensor

ABSTRACT

Nonstoichiometric nanocrystalline $LaFe_xO_{3-\delta}$ ($x = 0.7/0.8/0.9/1.0/1.1/1.2/1.3$) powers were prepared by sol–gel method with citric acid. Temperature dependence of resistance for $LaFe_xO_{3-\delta}$ sensors fits best to Holsteins model of small polaron hopping conduction. The resistance is determined by the competition between electrical valence compensation and oxygen vacancy compensation. And at each fixed temperature, the resistance is decreased with the introduction of more Fe deficiency. XPS analysis on O1s and C1s spectra verifies the existence of La-carbonate on the surface. The variation of surface concentration of adsorbed oxygen and La-carbonate, atomic ratio of Fe^{4+}/Fe^{3+} and Fe/La with x value are discussed in combination, which indicate that the release of electrons trapped by native active oxygen due to the decomposition of monodentate La-carbonate also makes contribution to the response of $LaFe_xO_{3-\delta}$ sensors to ethanol, in addition to the major contribution from adsorbed oxygen species. The best sensing performance of nanocrystalline $LaFe_{0.8}O_{3-\delta}$ sensor is ascribed to its relatively large surface concentration of adsorbed oxygen species and monodantate La-carbonate.

1. Introduction

Gas sensors based on $LaFeO_3$ nanoparticles have attracted considerable interests due to their high sensitivity and stability to ethanol and tunable selectivity to various gas by the substitution of cation ions [1–16]. Among various methods that can be used to prepare $LaFeO_3$ nanoparticles, sol–gel method using citric acid has been frequently adopted due to the low cost of raw materials and easy handle of procedures. However, the high resistance of the obtained nanoparticles limits the practical application.

For $LaFeO_3$, its charge carriers are holes produced by the ionization of the La^{3+} cation vacancy defect [17,18]. In order to keep charge neutrality, the substitution of trivalent La or Fe ions by bivalent cation element would lead to the increase of hole concentration by electric valence compensation or decrease of hole concentration by oxygen vacancy compensation. Mangy groups have reported that the partial substitution of La or Fe by lower valent cation elements such as Pb, Mg, Ba, Co, Sr and Ca could reduce the resistance of $LaFeO_3$-based sensors [1–3,5–11,16] by the competition of electric valence and oxygen vacancy compensation. Moreover, the sensing performance to ethanol has also been improved, which is often ascribed to smaller crystallite size and larger amount of adsorbed oxygen species (O_2^- or O^-) [5,10].

It is well known that the sensing properties of nanocrystalline $LaFeO_3$-based sensors are greatly related to oxygen adsorption [1,10]. The oxygen molecules adsorbed on the surfaces of nanograins could capture electrons from $LaFeO_3$, and results in the decrease of resistance of p-type $LaFeO_3$ [19]. However, the surface of lanthanum oxide samples prepared with citric acid would be enriched with carbonate species due to the reaction of CO_2 produced by the combustion process with the lanthanum oxide surface [20–24], therefore, the existence of surface carbonate species which has been neglected should also be considered when exploring the gas sensing mechanism of $LaFeO_3$-based sensors.

In addition to the common means of substitution of cation ions, we speculate that the introduction of intrinsic cation deficiency could be an alternative way to reduce the electrical resistance of perovskite oxides, and thus affect the sensing performance. Therefore, in the present work, we systematically investigated the influence of nonstoichiometry on the electrical transport and ethanol sensing properties of nanocrystalline $LaFe_xO_{3-\delta}$ powders which were prepared by sol–gel method with citric acid, and propose a combined ethanol sensing mechanism by the analysis of

* Corresponding author. Fax: +86 351 6018030.
E-mail address: caoensi@163.com (K. Cao).

http://dx.doi.org/10.1016/j.snb.2016.02.096
0925-4005/

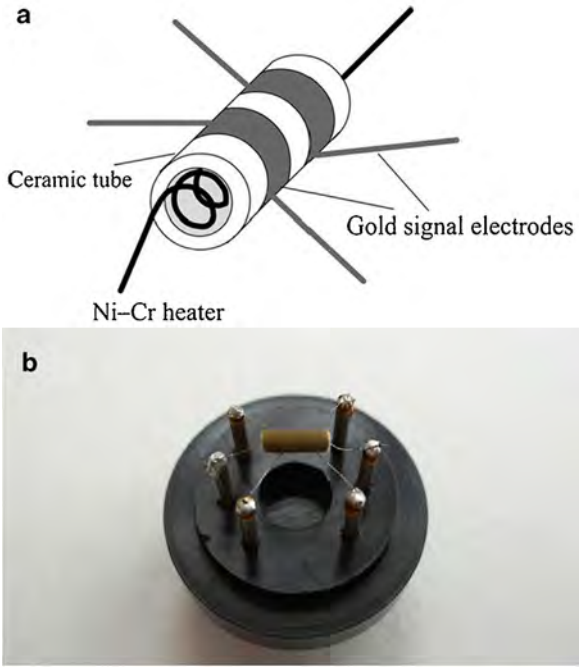

Fig. 1. (a) Schematic image of the sensor structure and (b) a photograph of the sensor.

XPS results, with the consideration of both oxygen adsorption and carbonate formation at the surface region.

2. Experimental

2.1. Preparation of powders

$LaFe_xO_{3-\delta}$ (x = 0.7/0.8/0.9/1.0/1.1/1.2/1.3) powders were prepared by a sol–gel method. Firstly, appropriate amount of $La(NO_3)_3{\cdot}6H_2O$, $Fe(NO_3)_3{\cdot}9H_2O$ and citric acid (all analytically pure) were dissolved in ion-free water at 80 °C. The polyethylene glycol (PEG) was added into the mixed solution under stirring at 80 °C to obtain the sol and the sol was dried to form gel. Then, gel pieces were formed through combustion process, and were ground to form fine powders. Finally, the fine powders were annealed at 600 °C for 2 h in an oven.

2.2. Characteristics of powders

X-ray diffraction patterns of the obtained $LaFe_xO_{3-\delta}$ powders were measured by X-ray diffractometer (D/max 2500, Rigaku Corporation, Japan) using Cu Kα radiation. X-ray photoelectron spectroscopy (XPS) measurements for $LaFe_xO_{3-\delta}$ nanocrystalline powders were performed with monochromated Al Kα radiation using X-ray photoelectron spectrometer (ESCALAB 250, Thermo Electron Corporation, USA).

2.3. Fabrication and measurements of sensors

0.1 g powders obtained above were mixed with 0.1 ml terpineol to form a paste. The sensors were made by coating ceramic tube (outside diameter = 1.2 mm, length = 4 mm) with the paste to form a thin sensing film, then annealed at 600 °C for 2 h in an oven to increase stability. A pair of gold electrodes was installed at each end of the ceramic tube before it was coated with the paste; each electrode was connected with two Pt wires. A Ni–Cr heating wire (diameter = 0.5 mm, resistance = 35 Ω) was inserted into the tube to form an indirect-heated gas sensor. Fig. 1(a) and (b) show the schematic image of the sensor structure and a photograph of the sensor, respectively. The electrical properties of the sensor were measured by an Intelligent Gas Sensing Analysis System (CGS-8, Beijing Elite Tech Co., Ltd., China). The sensor sensitivity was defined as the ratio (S = Rg/Ra) of the resistance of the sensor in target gases (Rg) and that in dry air (Ra). The operating temperature of the sensor was varied between 130 and 200 °C. The response and recovery time were defined as the time taken by the sensor to achieve 90% of the total resistance change in the case of adsorption and desorption, respectively.

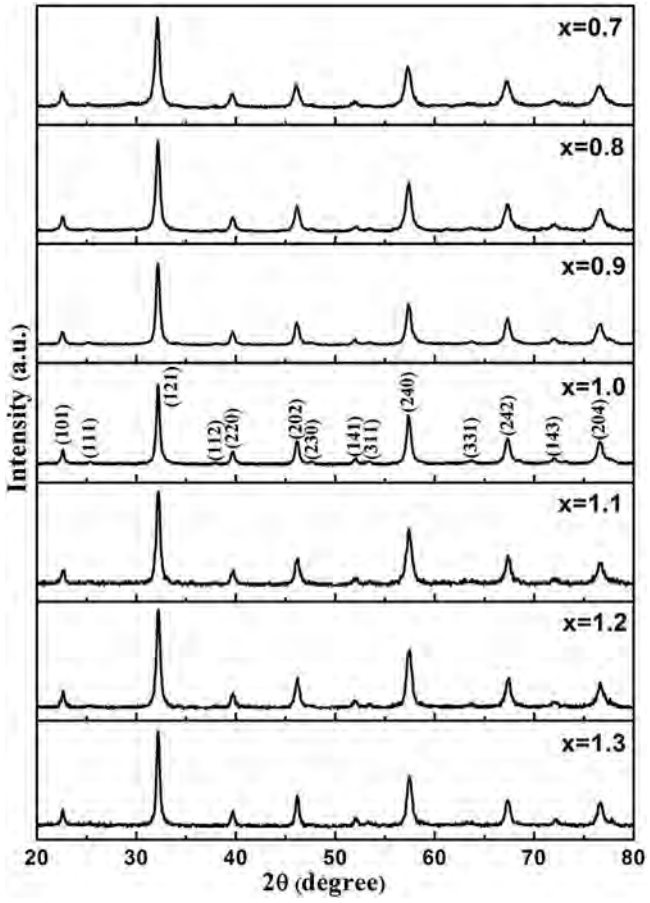

Fig. 2. X-ray diffraction patterns of $LaFe_xO_{3-\delta}$ powers annealed at 600 °C with different x value.

3. Results and discussion

3.1. Structural analysis

Fig. 2 shows the X-ray diffraction patterns of $LaFe_xO_{3-\delta}$ powers annealed at 600 °C with different x value. All the samples have a single phase with orthorhombic perovskite structure (space group Pnma-62), without any trace of impurity phase. Their lattice parameters, unit cell volumes, and average crystallite sizes are summarized in Table 1. The lattice parameters were calculated from peak positions and miller indices using Bragg law $2d\sin\theta = n\lambda$ and $1/d^2 = h^2/a^2 + k^2/b^2 + l^2/c^2$, where d is the interplanar spacing, h k and l are miller indices, a b and c are lattice parameters. Each lattice parameter changes with x values in its own way. The unit cell volume is calculated by the product of a b and c. Compared to the sample with x = 1.0, the unit cell volumes for the sample with x < 1.0 are larger, while the ones for the sample with x > 1.0 are smaller, indicating that the introduction of Fe deficiency results in the expansion of unit cell, while the introduction of La defi-

Table 1
Lattice parameters and average grain sizes for nanocrystalline $LaFe_xO_{3-\delta}$.

x	a (Å)	b (Å)	c (Å)	V (Å^3)	D (nm)
0.7	5.5802	7.87116	5.56282	244.33	14.1
0.8	5.56008	7.87294	5.56697	243.69	16.1
0.9	5.56545	7.87388	5.56873	244.03	18.0
1.0	5.55873	7.87264	5.56804	243.67	21.0
1.1	5.54915	7.87101	5.56617	243.16	20.2
1.2	5.56383	7.86039	5.55848	243.09	17.8
1.3	5.57014	7.85449	5.55810	243.17	17.3

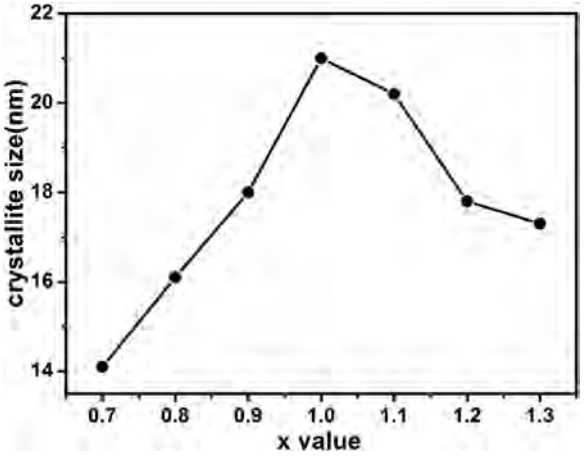

Fig. 3. Variation of mean crystallite size with x value for $LaFe_xO_{3-\delta}$ powers.

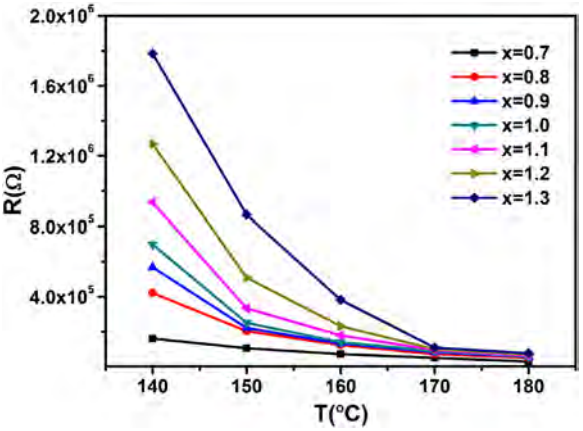

Fig. 4. Temperature dependence of resistance in air for $LaFe_xO_{3-\delta}$ sensors with different x value.

ciency leads to the contraction of unit cell. The crystallite size is estimated using the Scherrer formula $D = 0.89\lambda/\beta\cos\theta$, where D is the mean crystallite size, λ is the wavelength of the X-ray radiation (λ = 0.154 nm for Cu Kα1 radiation), and β is the full width at half-maximum of diffraction peak at 2θ [25]. As shown in Fig. 3, the introduction of La or Fe deficiency both results in the reduce of crystallite size, among which the introduction of Fe deficiency is more efficient.

3.2. Electrical properties

The temperature dependence of resistances in air for nanocrystalline $LaFe_xO_{3-\delta}$ sensors are shown in Fig. 4. The resistance of all samples decreases with an increase of temperature, exhibiting semiconducting behavior. In addition, at each fixed operating temperature, the resistance of $LaFe_xO_{3-\delta}$ sensors decreases with the decrease of x value from 1.3 to 0.7.

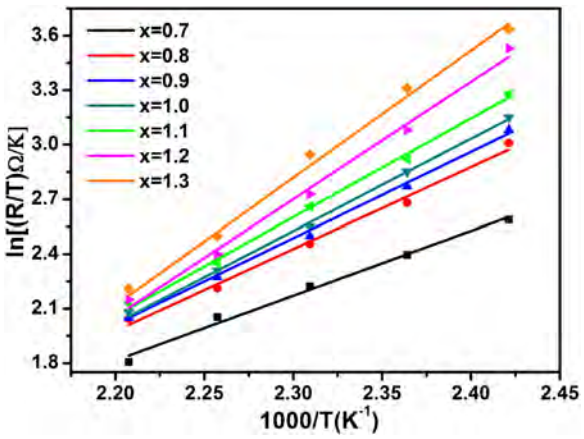

Fig. 5. ln[R/T] vs. 1000/T curve for $LaFe_xO_{3-\delta}$ sensors with different x value.

For bulk $LaFeO_3$, its charge carriers are holes produced by the ionization of the La^{3+} cation vacancy defect. When Fe or La deficiency is introduced, in order to maintain the charge neutrality, both electrical valence compensation and oxygen vacancy compensation could occur.

With the decrease of x value, more Fe^{4+} ions would be transformed from Fe^{3+} ions. These Fe^{4+} ions could provide some holes in the compound and prefer an increase of conductivity. On the other side, oxygen vacancies could provide some electrons in the compound, which compensate part of holes and prefer an increase of resistance. As a matter of fact, the resistance is determined by the compound compensation processes with the competition of electrical valence and oxygen vacancy compensation. Therefore, it is reasonable to write $LaFe_xO_{3-\delta}$ to denote our samples.

As shown in Fig. 5,the resistance R of all the samples fits best to Holsteins model of small polaron hopping conduction [26–28]:

$$R(T) = R_0 T \exp\left(\frac{E_a}{k_B T}\right)$$

with $E_a = E_H + E_D/2$ for $T > \Theta_D/2$, and $E_a = E_D$ for $T < \Theta_D/4$ in the measurement range of temperature from 140 °C to 180 °C, where E_a is activation energy, k_B is the Boltzmann constant, Θ_D is Deby temperature, E_H is the hopping energy and E_D is the disorder energy (the difference of electronic energies between two hopping sites). The result is in agreement with the works by Liu et al. [2], Shi et al. [10], Khetre et al. [29], and Murade et al. [30], who suggested that small polarons hopping is responsible for the electronic conduction in $LaFeO_3$ [31–34]. The presence of small polarons implies the existence of local lattice distortions which localize the charge carriers.

The variation of E_a with x value for $LaFe_xO_{3-\delta}$ sensors with different x value is displayed in Fig. 6. Compared to the sample with x = 1.0, E_a becomes smaller through the introduction of more Fe deficiency, whereas E_a becomes larger through the introduction of more La deficiency. Therefore, the reason that the introduction of more Fe deficiency results in the decrease of resistance is in essence due to the reduction of E_a, which makes the hopping of small polarons much easier.

3.3. Gas-sensing properties and mechanism

The operating temperature dependence of sensitivity to 1000 ppm ethanol for nanocrystalline $LaFe_xO_{3-\delta}$ sensors is shown in Fig. 7. With increasing operating temperature, the sensitivity of $LaFe_xO_{3-\delta}$ sensors increases at first, undergoes a maximum at 140 °C, and then decreases again. Meanwhile, the sensitivity of $LaFe_xO_{3-\delta}$ sensors at each fixed temperature increases with

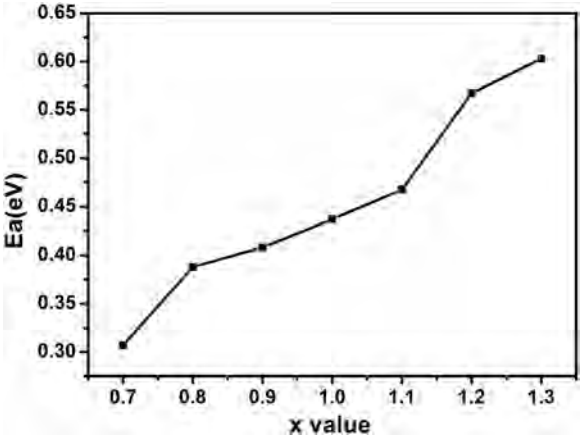

Fig. 6. Variation of E_a with x value for $LaFe_xO_{3-\delta}$ sensors with different x value.

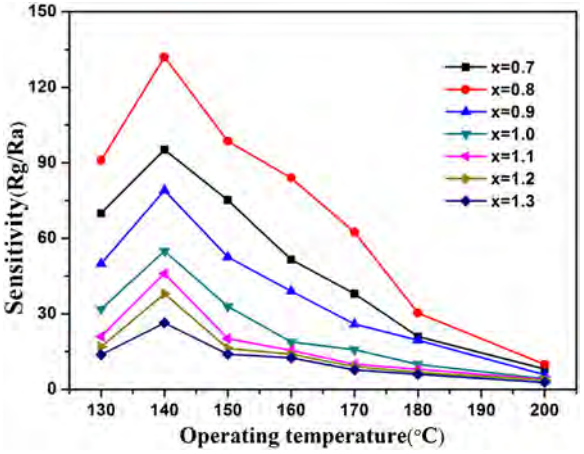

Fig. 7. Operating temperature dependence of sensitivity to 1000 ppm ethanol for nanocrystalline $LaFe_xO_{3-\delta}$ sensors.

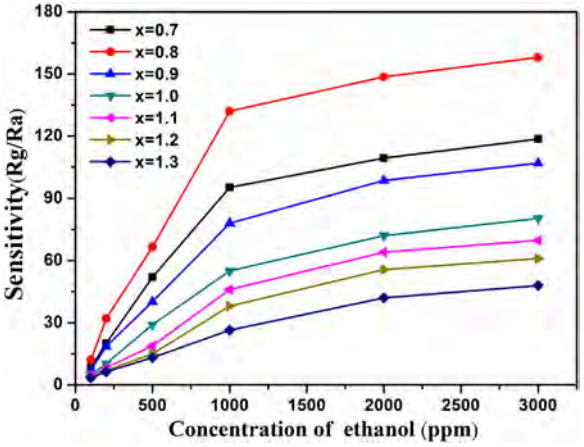

Fig. 8. Sensitivity of nanocrystalline $LaFe_xO_{3-\delta}$ sensors to different concentration of ethanol at 140 °C.

decreasing x value, reaches a maximum at $x = 0.8$, and decreases again at $x = 0.7$, the sensitivity of which is still larger than that of $x = 0.9$. The best sensitivity to 1000 ppm ethanol is 132 obtained at 140 °C by the sample with $x = 0.8$.

Fig. 8 displays the sensitivity of nanocrystalline $LaFe_xO_{3-\delta}$ sensors to different concentration of ethanol at 140 °C. The sensitivity of each sensor increases fast with increasing concentration of ethanol in the range of 100–1000 ppm, while the increase rate

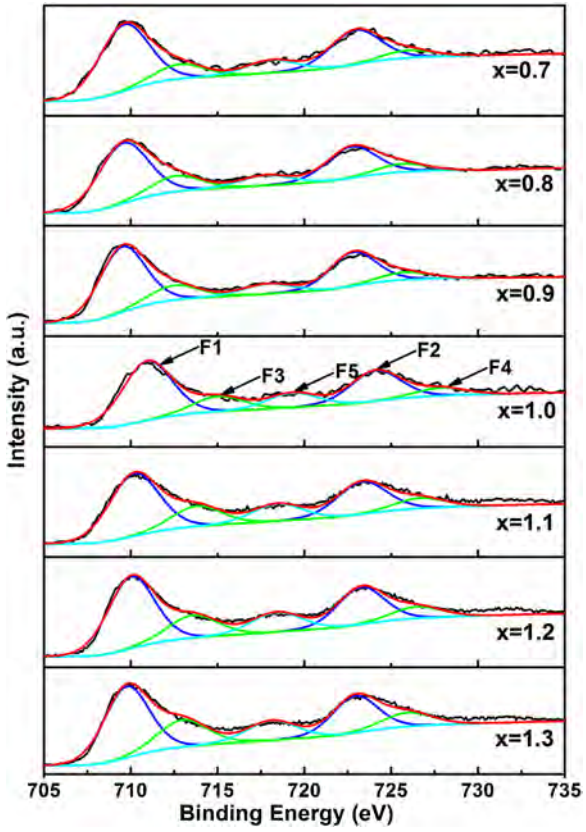

Fig. 9. The Fe2p XPS for nanocrystalline $LaFe_xO_{3-\delta}$ with different x value.

becomes relatively slow in the range of 1000–3000 ppm due to the limited active adsorption sites at the surface of each sensor.

Since the sensing properties of perovskite nanopowders are greatly related with the surface characteristics, surface-sensitive XPS was carried out to determine the surface composition and valence state of each element in nonstoichiometric $LaFe_xO_{3-\delta}$.

Fig. 9 shows the Fe2p XPS with peak deconvolutions for nanocrystalline $LaFe_xO_{3-\delta}$. The doublet peaks of F1 and F2 could be assigned to $2p_{3/2}$ and $2p_{1/2}$ states of Fe^{3+}, meanwhile the doublet peaks of F3 and F4 could be assigned to $2p_{3/2}$ and $2p_{1/2}$ states of Fe^{4+}, and peak of F5 is a satellite [10,16]. However, no peaks corresponding to Fe^{2+} ions could be observed for our nanocrystalline $LaFe_xO_{3-\delta}$ with $x \geq 1$, indicating that Fe^{2+} ions are not present at the detected surface region.

Fig. 10 shows the La3d XPS with peak deconvolutions for nanocrystalline $LaFe_xO_{3-\delta}$. The doublet peaks of L1 and L2 could be assigned to $3d_{5/2}$ and $3d_{3/2}$ states of La final state without charge transfer, also denoted $c4f^0$ (c indicates the presence of a core hole, $4f^0$ the absence of electrons in the 4f orbital), meanwhile the satellite peaks of L3 and L4 as well as the satellite peaks of L5 and L6 could be assigned to antibonding and bonding component of the final state with charge transfer, denoted $c4f^1L$ to mark the transfer of an electron from the ligand atom L to the 4f orbital. The peak of L7 is ascribed to $3d_{5/2}$ plasmons [35]. These data indicate that lanthanum ions are present in the trivalent form for all the samples.

As shown in Fig. 11, the O1s XPS signal can be divided into two peaks, corresponding to two kinds of oxygen at the surface. The lower BE peak of O1 is generally assigned to lattice oxygen species in $LaFeO_3$, and the higher BE peak of O2 is ascribed to the adsorbed oxygen (O_{ads}) [10,16]. As for the sample with $x = 0.8$ and $x = 1.1$, perfect fitting of O1s spectrum requires a third peak of O3 at even higher BE. In combination with the C1s analysis, the peak of O3 is

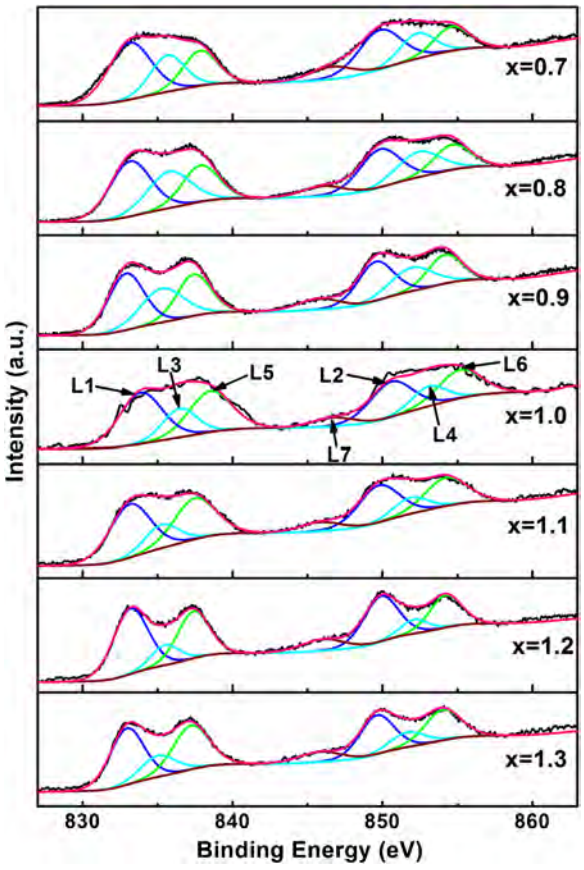

Fig. 10. The La3d XPS for nanocrystalline $LaFe_xO_{3-\delta}$ with different x value.

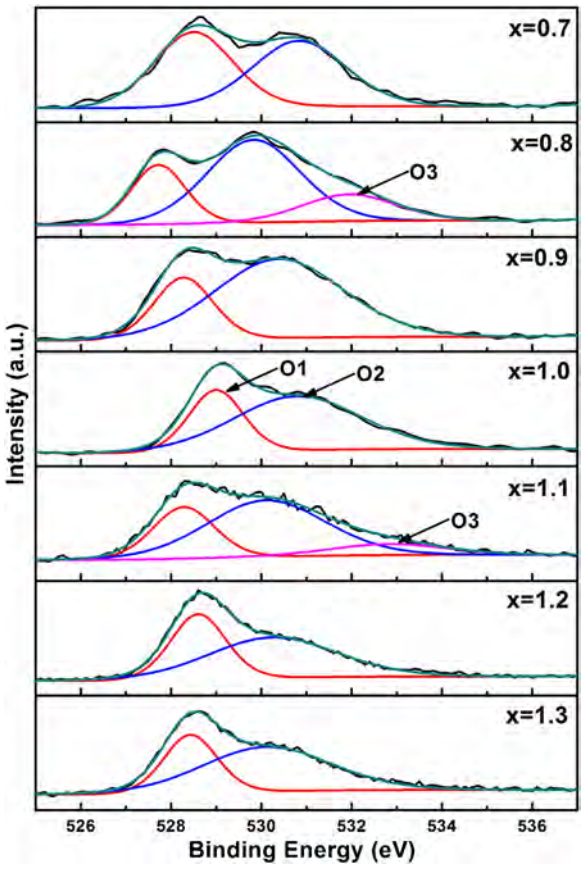

Fig. 11. The O1s XPS for nanocrystalline $LaFe_xO_{3-\delta}$ with different x value.

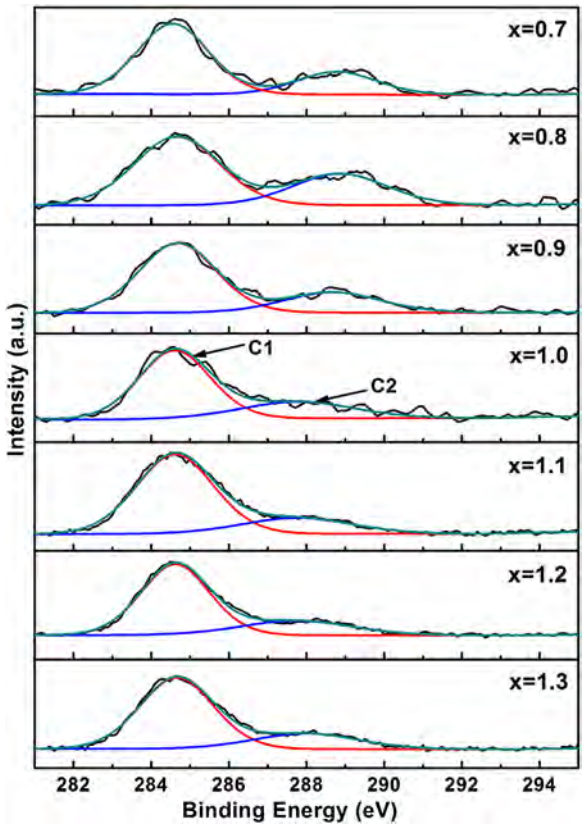

Fig. 12. The C1s XPS for nanocrystalline $LaFe_xO_{3-\delta}$ with different x value.

ascribed to the oxygen that links La– and $-CO_2$ in monodentate La-carbonate La–O–CO_2.

In addition, the surface composition of perovskite nanopowders is significantly affected by the gases in contact with the solid during synthesis. The surface of lanthanum oxide samples [20–24] prepared with citric acid was reported to be enriched with carbonate species due to the reaction of CO_2 produced by the combustion process with the lanthanum oxide surface. According to the propellant chemistry [36] and following the works of many other researchers [24], the global redox reactions between lanthanum and iron nitrates to form $LaFe_xO_{3-\delta}$ in the presence of citric acid can be written as:

$$La(NO_3)_3{\cdot}6H_2O(c)+(x)Fe(NO_3)_3{\cdot}9H_2O(c)+C_6H_8O_7(c)\rightarrow$$
$$LaFe_xO_{3-\delta}(c)+[(3+3x)/2]N_2(g)+(6)CO_2(g)+[(9x-3+\delta)/2]O_2(g)+(10+9x)H_2O(g)$$

CO_2, H_2O and N_2 were considered as the most stable products of the combustion synthesis with respect to other theoretical acceptable combinations that might be considered, including the formation of nitrogen oxides, CO and so forth. Therefore, La-carbonates could be formed due to the reaction of the evolved CO_2 gas with superficial La–O sites at the high local temperature under the combustion reaction.

Inspection of the C1s region in Fig. 12 reveals that, besides adventitious carbon (peak C1) which is used as reference, a small amount of carbonates (peak C2) has indeed accumulated at the surface region of nanocrystalline $LaFe_xO_{3-\delta}$[23,24].

The variation of surface concentration of adsorbed oxygen (O_{ads}) and carbonate with x value are shown in Fig. 13. Since monodentate La-carbonate could be formed at the surface of all the samples, the peak of O2 for samples with x = 0.7/0.9/1.0/1.2/1.3 could also have contribution from La-carbonate other than adsorbed oxygen. Therefore, the calculation of the surface concentration of adsorbed oxygen (O_2^- or O^-) requires the removal of O1s signal from monodentate La-carbonate by subtraction of carbonate concentration

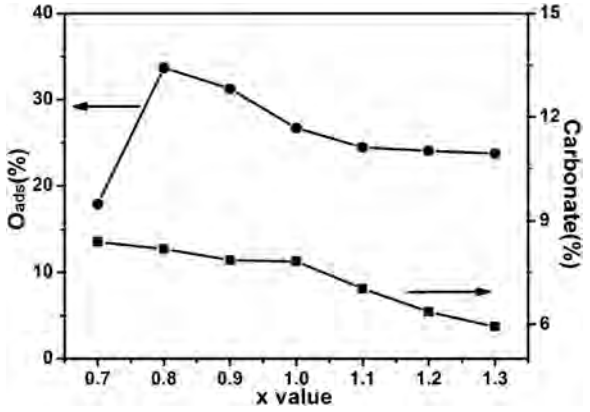

Fig. 13. Variation of surface concentration of adsorbed oxygen (O_{ads}) and carbonate with x value for nanocrystalline $LaFe_xO_{3-\delta}$.

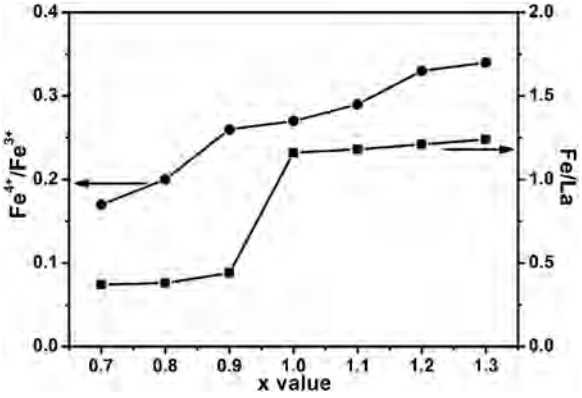

Fig. 14. Variation of atomic ratio of Fe^{4+}/Fe^{3+} and Fe/La with x value for nanocrystalline $LaFe_xO_{3-\delta}$.

(C2). Compared to 26.71% for the sample with $x = 1.0$, the concentration of O_{ads} increases with more Fe deficiency, reaching its maximum of 33.69% at $x = 0.8$, then drops to its minimum of 17.85% at $x = 0.7$. With regard to the small concentration of O_{ads} for the sample with $x = 0.7$, we speculate that a small amount of La_2O_3 might be liberated from $LaFe_xO_{3-\delta}$ lattice, and La_2O_3 could not provide adsorption site for oxygen molecule.

As for the concentration of carbonate, it decreases monotonously from 8.39% at $x = 0.7$ to 5.93% at = 1.3, indicating that more La^{3+} cations faciliate the formation of carbonates, and the carbonate species should be La-carbonates due to the strong basic character of La^{3+} cations. With regard to the sample with $x = 0.7$, La-carbonate could also be formed at the surface of La_2O_3, thus the concentration of carbonate is related with La ions. The calcination at 600 °C for 2 h before characterization would result in CO_2 desorption from La-carbonate species, therefore the present La-carbonate on the surface should be monodentate carbonate due to its easier formation and higher thermal stability than bidentate carbonate [37]. The formation of monodentate La-carbonate La–O–CO_2 requires one CO_2 molecule and one superficial La–O site, and would lead to the electron transfer from CO_2 to oxygen.

The surface layers of perovskite nanopowders could display different atomic concentrations with respect to the bulk. For ideally stoichiometric bulk $LaFeO_3$, all La and Fe ions belong to Fe^{3+}. However, on the basis of XPS analysis, the calculated atomic ratio of Fe^{4+}/Fe^{3+} is 0.27, and the atomic ratio of Fe/La is 1.16 for our $LaFe_xO_{3-\delta}$ with $x = 1.0$. In order to maintain the material to be charge neutrality, the La vacancies in $LaFeO_3$ may induce Fe^{4+} or oxygen vacancy. If the charge compensation was all caused by the formation of Fe^{4+}, the theoretical atomic ratio of Fe^{4+}/Fe^{3+} for our $LaFeO_3$ should be 0.16, much smaller than the value of 0.27. When oxygen vacancy compensation was considered, the concentration of Fe^{4+} would be reduced, and atomic ratio of Fe^{4+}/Fe^{3+} would be even smaller. According to ab initio calculation [19], the electron transfer from Fe ion to adsorbed oxygen could result in the transformation from Fe^{3+} to Fe^{4+} at some Fe site. Therefore, oxygen adsorption should be considered besides charge and oxygen vacancy compensation.

The variation of atomic ratio of Fe^{4+}/Fe^{3+} and Fe/La with x value for nanocrystalline $LaFe_xO_{3-\delta}$ are displayed in Fig. 14. The atomic ratio of $Fe^{4+}/Fe^{3+}$and Fe/La both increase with increasing x value. Compared to the sample with $x = 1.0$, the introduction of more Fe deficiency with $x < 1$ results in decreased concentration of Fe^{4+} ions, and the atomic ratio of Fe/La is much smaller than designed, making the surface a La-rich region. With the decrease of x value, the atomic ratio of Fe/La decreases, more La ions would be exposed to air, thus the proportion of oxygen adsorbed at Fe site would be reduced, leading to less transformation from Fe^{3+} to Fe^{4+}, and thus decreased atomic ratio of Fe^{4+}/Fe^{3+}. On the other side, the introduction of more La deficiency with $x \geq 1$ results in increased concentration of Fe^{4+} ions, and the atomic ratios of Fe/La are all above 1, making the surface a Fe-rich region. For $LaFe_xO_{3-\delta}$ with $x \geq 1$, as discussed above, La deficiency would result in the partial transformation of Fe^{3+} ions into Fe^{4+} ions. With the increase of x value, more Fe^{4+} ions would be formed to maintain charge neutrality. In addition, more Fe ions would be exposed to air for Fe-rich sample, thus the proportion of oxygen adsorbed at Fe site would be increased, resulting in more transformation from Fe^{3+} to Fe^{4+}.

With increasing temperature in air, the oxygen species adsorbed on the surface of $LaFe_xO_{3-\delta}$ undergoes the following reactions:

$$O_{2(gas)} \leftrightarrow O_{2(ads)} \quad (a)$$

$$O_{2(ads)} + e^- \leftrightarrow O^-_{2(ads)} \quad (b)$$

$$O^-_{2(ads)} + e^- \leftrightarrow 2O^-_{ads} \quad (c)$$

$$O^-_{ads} + e^- \leftrightarrow O^{2-}_{ads} \quad (d)$$

The equilibrium shifts to the right with an increase of operating temperature. The adsorbed oxygen (O_2^- or O^-) captures electrons from $LaFe_xO_{3-\delta}$, leading to an increase of hole concentration. In addition, CO_2 desorption would take place due to the decomposition of monodentate La-carbonate in the temperature range of 100–150 °C [37], resulting in increased concentration of native active oxygen ($O^-_{(native)}$) in the presence of oxygen.

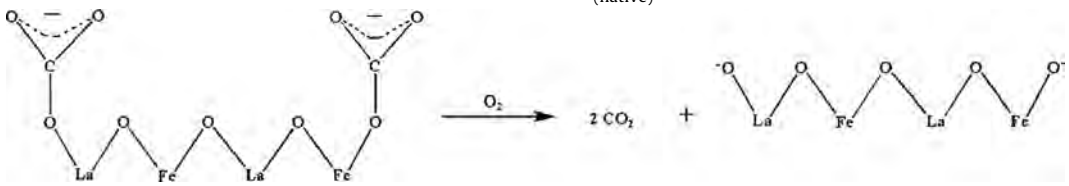

When ethanol is introduced, the following reactions may happen:

$$C_2H_5OH + 6O^{n-}_{(ads)} \rightarrow 2CO_2 + 3H_2O + 6ne^- \quad (a)$$

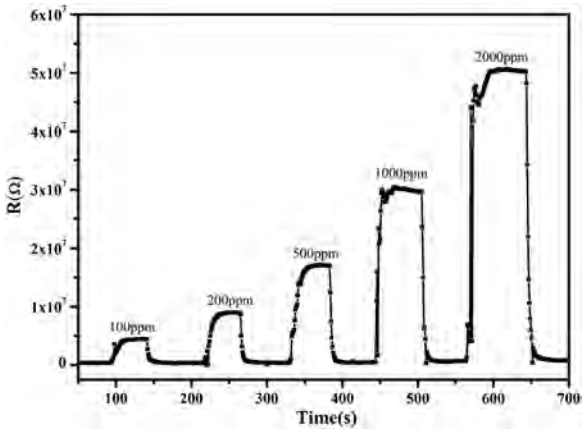

Fig. 15. Dynamic response of resistance to different concentration of ethanol for nanocrystalline $LaFe_{0.8}O_{3-\delta}$ sensor at 140 °C.

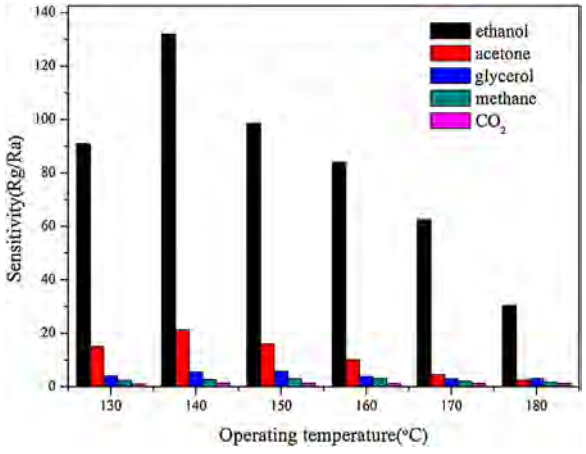

Fig. 16. Sensitivity of nanocrystalline $LaFe_{0.8}O_{3-\delta}$ sensor to 1000 ppm different gases at 130–180 °C.

$$C_2H_5OH + 6O^-_{(native)} \rightarrow 2CO_2 + 3H_2O + 6e^- \quad (b)$$

The electrons trapped by the adsorbed oxygen species from air and native active oxygen $O^-_{(native)}$ are released to semiconductor, leading to a decrease of holes, thus an increase in resistance of semiconductor sensor. Therefore, the sensing performance of $LaFe_xO_{3-\delta}$ is greatly influenced by the surface concentration of adsorbed oxygen species (O_2^- or O^-) and native active oxygen ($O^-_{(native)}$). The best performance for the sample with $x = 0.8$ is ascribed to its large concentration of adsorbed oxygen and monodentate La-carbonate, as well as its small crystallite size. As for the sample with $x = 0.7$, although the concentration of adsorbed oxygen (O_2^- or O^-) was greatly reduced, the contribution from La-carbonate, La_2O_3 liberated from $LaFe_xO_{3-\delta}$ lattice and crystallite size might be responsible for the modification of its sensing performance.

Fig. 15 shows the dynamic response of resistance to different concentration of ethanol for nanocrystalline $LaFe_{0.8}O_{3-\delta}$ sensor at 140 °C. The resistance of the sensor can recover to its initial value when ethanol was taken out, displays good stability. The response and recover time were estimated as 1 s and 1.5 s to 1000 ppm ethanol, respectively. So far as we know, the response and recover time is the shortest ever reported.

Fig. 16 displays the sensitivity of nanocrystalline $LaFe_{0.8}O_{3-\delta}$ sensor to 1000 ppm different gases at 130–180 °C. The sensitivity to acetone, glycerol, methane, CO_2 is all below 22 in the temperature range of 130–180 °C, much smaller than the sensitivity to ethanol at each fixed temperature, exhibiting good selectivity of the sensor.

4. Conclusions

In the present work, we experimentally investigated the influence of nonstoichiometry on the electrical transport and ethanol sensing characteristics for nanocrystalline $LaFe_xO_{3-\delta}$ sensors. The temperature dependence of resistance for $LaFe_xO_{3-\delta}$ sensors obeys Holstein's model of small polaron hopping conduction. And the resistance is determined by the competition between electrical valence compensation and oxygen vacancy compensation.

XPS analysis verifies the existence of adsorbed oxygen species and La-carbonate on the surface. In addition, nonstoichiometry has great influence on the atomic ratio of Fe^{4+}/Fe^{3+}, surface concentration of adsorbed oxygen and La-carbonate. After comprehensive analysis, the response of $LaFe_xO_{3-\delta}$ sensors to ethanol is ascribed to the release of electrons trapped by the adsorbed oxygen species from air and by native active oxygen site due to the decomposition of monodentate La-carbonate at operating temperature, leading to a decrease of holes, thus an increase in resistance. The best sensitivity to 1000 ppm ethanol is 132 obtained by nanocrystalline $LaFe_{0.8}O_{3-\delta}$ sensor due to its relatively large surface concentration of adsorbed oxygen species and monodantate La-carbonate, which also displays fast response and recovery, good stability and selectivity to ethanol at relatively lower prime operating temperature.

In conclusion, the resistance of nanocrystalline $LaFe_xO_{3-\delta}$ is determined by its bulk properties, while the sensing characteristic is greatly related with its surface composition. Appropriate introduction of cation deficiency could be an efficient way to fulfill the aim of reduced resistance and enhanced sensing performance for perovskite oxides.

Acknowledgments

This work was supported by National Natural Science Foundation of China (11404236) and Natural Science Foundation of Shanxi (2014021018-2).

Appendix A. Supplementary data

Supplementary data associated with this article can be found, in the online version, at http://dx.doi.org/10.1016/j.snb.2016.02.096.

References

[1] L. Zhang, H. Qin, P. Song, J. Hu, M. Jiang, Electrical properties and acetone sensing characteristics of $La_{1-x}Pb_xFeO_3$ perovskite system, Mater. Chem. Phys. 98 (2006) 358–362.
[2] X. Liu, B. Cheng, H. Qin, P. Song, S. Huang, R. Zhang, J. Hu, M. Jiang, Preparation, electrical and gas-sensing properties of perovskite-type $La_{1-x}Mg_xFeO_3$ semiconductor materials, J. Phys. Chem. Solids 68 (2007) 511–515.
[3] X. Liu, B. Cheng, J. Hu, H. Qin, M. Jiang, Semiconducting gas sensor for ethanol based on $LaMg_xFe_{1-x}O_3$ nanocrystals, Sens. Actuators B 129 (2008) 53–58.
[4] Y.G. Cho, K.H. Choi, Y.R. Kim, J.S. Jung, S.H. Lee, Characterization and catalytic properties of surface La-rich $LaFeO_3$ perovskite, Bull. Korean Chem. Soc. 30 (2009) 1368–1372.
[5] L.H. Sun, H.W. Qin, K.Y. Wang, M. Zhao, J.F. Hu, Structure and electrical properties of nanocrystalline $La_{1-x}Ba_xFeO_3$ for gas sensing application, Mater. Chem. Phys. 125 (2011) 305–308.
[6] C.H. Feng, S.P. Ruan, J.J. Li, B. Zou, J.Y. Luo, W.Y. Chen, W. Dong, F.Q. Wu, Ethanol sensing properties of $LaCo_xFe_{1-x}O_3$ nanoparticles: effects of calcination temperature, Co-doping, and carbon nanotube-treatment, Sens. Actuators B 155 (2011) 232–238.
[7] C. Doroftei, P.D. Popa, F. Iacomi, Synthesis of nanocrystalline La–Pb–Fe–O perovskite and methanol-sensing characteristics, Sens. Actuators B 161 (2012) 977–981.
[8] K. Fan, H. Qin, L. Wang, L. Ju, J. Hu, CO2 gas sensors based on $La_{1-x}Sr_xFeO_3$ nanocrystalline powders, Sens. Actuators B 177 (2013) 265–269.
[9] P.J. Yao, J. Wang, W.L. Chu, Y.W. Hao, Preparation and characterization of $La_{1-x}Sr_xFeO_3$ materials and their formaldehyde gas-sensing properties, J. Mater. Sci. 48 (2013) 441–450.
[10] C. Shi, H. Qin, M. Zhao, X. Wang, L. Li, J. Hu, Investigation on electrical transport, CO sensing characteristics and mechanism for nanocrystalline $La_{1-x}Ca_xFeO_3$ sensors, Sens. Actuators B 190 (2014) 25–31.

[11] A. Benali, S. Azizi, M. Bejar, E. Dhahri, M.F.P. Graça, Structural, electrical and ethanol sensing properties of double-doping $LaFeO_3$ perovskite oxides, Ceram. Int. 40 (2014) 14367–14373.
[12] P. Song, H. Zhang, D. Han, J. Li, Z. Yang, Q. Wang, Preparation of biomorphic porous $LaFeO_3$ by sorghum straw biotemplate method and its acetone sensing properties, Sens. Actuators B 196 (2014) 140–146.
[13] H. Zhang, P. Song, D. Han, Q. Wang, Synthesis and formaldehyde sensing performance of $LaFeO_3$ hollow nanospheres, Phys. E 63 (2014) 21–26.
[14] H.X. Xiao, C. Xue, P. Song, J. Li, Q. Wang, Preparation of porous $LaFeO_3$ microspheres and their gas-sensing property, Appl. Surf. Sci. 337 (2015) 65–71.
[15] J. Qin, Z.D. Cui, X.J. Yang, S.L. Zhu, Z.Y. Li, Y.Q. Liang, Synthesis of three-dimensionally ordered macroporous $LaFeO_3$ with enhanced methanol gas sensing properties, Sens. Actuators B 209 (2015) 706–713.
[16] J. Qin, Z.D. Cui, X.J. Yang, S.L. Zhu, Z.Y. Li, Y.Q. Liang, Three-dimensionally ordered macroporous $La_{1-x}Mg_xFeO_3$ as high performance gas sensor to methanol, J. Alloys Compd. 635 (2015) 194–202.
[17] J. Mizusaki, M. Yoshihiro, S. Yamauchi, K. Fueki, Thermodynamic quantities and defect equilibrium in the perovskite-type oxide solid solution $La_{1-x}FeO_{3-\delta}$, J. Solid State Chem. 67 (1987) 1–8.
[18] J. Mizusaki, M. Yoshihiro, S. Yamauchi, K. Fueki, Nonstoichimetry and defect structure of the perovskite-type oxides $La_{1-x}Sr_xFeO_{3-\delta}$, J. Solid State Chem. 58 (1985) 257–266.
[19] X. Liu, J. Hu, B. Cheng, H. Qin, M. Zhao, C. Yang, First-principles study of O_2 adsorption on the LaFeO3 (0 1 0) surface, Sens. Actuators B 139 (2009) 520–526.
[20] J.C. Lavalley, Use of probe molecules for characterization of the surface basicity of divided metal oxides, Trends Phys. Chem. 2 (1991) 305–326.
[21] S. Bernal, J.A. Diaz, R. Garcia, J.M. Rodriguez-Izquierdo, Study of some aspects of the reactivity of La_2O_3 with CO_2 and H_2O, J. Mater. Sci. 20 (1985) 537–541.
[22] S. Bernal, F.J. Botana, R. Garcia, J.M. Rodriguez-Izquierdo, Behaviour of rare earth sesquioxides exposed to atmospheric carbon dioxide and water, React. Solids 4 (1987) 23–40.
[23] V.G. Milt, R. Spretz, M.A. Ulla, E.A. Lombardo, J.L. Garcia Fierro, The nature of active sites for the oxidation of methane on La-based perovskites, Catal. Lett. 42 (1996) 57–63.
[24] H. Najjar, H. Batis, La–Mn perovskite-type oxide prepared by combustion method: catalytic activity in ethanol oxidation, Appl. Catal. A: Gen. 383 (2010) 192–201.
[25] B.E. Warren, X-ray Diffraction, Addison–Wesley, Reading, MA, 1980, p. 253.
[26] J.M. De Teresa, K. Dörr, K.H. Müller, L. Schultz, Strong influence of the Mn^{3+} content on the binding energy of the lattice polarons in manganese perovskites, Phys. Rev. B 58 (1998) R5928–R5931.
[27] G.J. Snyder, R. Hiskes, S. DiCarolis, M.R. Beasley, T.H. Geballe, Intrinsic electrical transport and magnetic properties of $La_{0.67}Ca_{0.33}MnO_3$ and $La_{0.67}Sr_{0.33}MnO_3$ MOCVD thin film and bulk material, Phys. Rev. B 53 (1996) 14434–14444.
[28] X.D. Zhou, Q. Cai, J. Yang, M. Kim, W.B. Yelon, W.J. James, Y.W. Shin, B.J. Scarfinio, H. Anderson, Coupled electrical and magnetic properties in (La, Sr)$FeO_{3-\delta}$, J. Appl. Phys. 97 (2005) 10C314.
[29] S.M. Khetre, H.V. Jadhav, P.N. Jagadale, S.R. Kulal, S.R. Bamane, Studiesonelectrical and dielectrical properties of $LaFeO_3$, Adv. Appl. Sci. Res. 2 (2011) 503–511.
[30] P.A. Murade, V.S. Sangawar, G.N. Chaudhari, V.D. Kapse, A.U. Bajpeyee, Acetone gas-sensing performance of Sr-doped nanostructured $LaFeO_3$ semiconductor prepared by citrate sol–gel route, Curr. Appl. Phys. 11 (2011) 451–456.
[31] J.B. Goodenough, Metallic Oxides Progress Solid State Chemistry, vol. 5, Pergamon, Oxford, 1971, pp. 145–399.
[32] E. Iguchi, W.H. Jung, Electrical transports of $LaFe_{1-x}Ti_xO3$ ($x \leq 0.10$), J. Physical Soc. Jpn. 63 (1994) 3078–3086.
[33] J. Mizusaki, T. Sasamoto, W.R. Cannon, H.K. Bowen, Electronic conductivity, seebeck coefficient, and defect structure of $LaFeO_3$, J. Am. Ceram. Soc. 65 (1982) 363–368.
[34] K.K. Bhargav, S. Ram, S.B. Majumder, Small polaron conduction in lead modified lanthanum ferrite ceramics, J. Alloys Compd. 638 (2015) 334–343.
[35] M.F. Sunding, K. Hadidi, S. Diplas, O.M. Løvvik, T.E. Norby, A.E. Gunnæs, XPS characterization of in situ treated lanthanum oxide and hydroxide using tailored charge referencing and peak fitting procedures, J. Electron Spectrosc. Rel. Phenom. 184 (2011) 399–409.
[36] S.R. Jain, K.C. Adiga, V.R. Pai Verneker, A new approach to thermochemical calculations of condensed fuel-oxidizer mixtures, Combus. Flame 40 (1981) 71–79.
[37] V. Cortes Corberan, Luis G. Tejuca, Alexis T. Bell, Surface reactivity of reduced $LaFeO_3$ as studied by TPD and IR spectroscopies of CO, CO_2 and H_2, J. Mater. Sci. 24 (1989) 4437–4442.

Biographies

Kang Cao is currently working toward the MS degree at College of Physics & Optoelectronics, Taiyuan University of Technology, China. His research focuses on the synthesis of new functional nanostructure materials and their application in gas sensors.

Ensi Cao received his Ph.D. degree in materials physics and chemistry, Shandong University, in 2012. Currently, he is a lecturer at College of Physics & Optoelectronics, Taiyuan University of Technology. His current fields of interest are magnetic materials, multiferroics materials, low-dimensional materials and gas sensors.

Yongjia Zhang received his Ph.D. degree in materials physics and chemistry, Shandong University, in 2013. Currently, he is a lecturer at College of Physics & Optoelectronics, Taiyuan University of Technology. His current fields of interest are magnetic materials, multiferroics materials, low-dimensional materials and gas sensors.

Wentao Hao received his Ph.D. degree in condensed physics, Shandong University, in 2012. Currently, he is a lecturer at College of Physics & Optoelectronics, Taiyuan University of Technology. His current fields of interest are functional ceramics, low-dimensional materials and gas sensors.

Li Sun received his Ph.D. degree in condensed physics, Shandong University, in 2012. Currently, he is a lecturer at College of Physics & Optoelectronics, Taiyuan University of Technology. His current fields of interest are magnetic materials, multiferroics materials, low-dimensional materials and gas sensors.

Hua Peng received her Ph.D. degree in condensed physics, Shandong University, in 2012. Currently, she is a lecturer at College of Physics & Optoelectronics, Taiyuan University of Technology. Her current fields of interest are thermoelectric materials and gas sensors.